Spectroscopic Study of Film Formation From Polystyrene Latex/TiO_2 Nanocomposites Prepared by Dip-Coating Method

M. Selin Sunay,[1] Onder Pekcan,[2] Md. Mahbubor Rahman,[3] Abdelhamid Elaissari,[3] Saziye Ugur[1]
[1] *Department of Physics, Istanbul Technical University, Maslak 34469, Istanbul, Turkey*

[2] *Kadir Has University, Cibali 34320, Istanbul, Turkey*

[3] *University of Lyon, Villeurbanne, LAGEP, UMR-5007@CPE, 43 bd 11 Nov. 1918, F-69622, France*

In this study, we investigated the influence of TiO_2 content and thickness of polystyrene (PS) template on film-formation behavior of PS/TiO_2 composites using fluorescence and ultraviolet–visible techniques in conjunction with scanning electron microscopy. Films were prepared by coating PS templates with various layers of TiO_2 using dip-coating method. The results showed that PS latexes present complete film formation on top surface of composites. After extraction of PS, a well-defined interconnected porosity were obtained for thin films when TiO_2 content was increased, whereas thick samples did not present any interconnected porous structures above a certain TiO_2 layer. POLYM. ENG. SCI., 54:288–302, 2014. © 2013 Society of Plastics Engineers

INTRODUCTION

Polymer latexes are being used in a broad range of fields from adhesives, inks, paints, coatings, drug delivery systems, and films to cosmetics [1]. In many of these applications, latexes form thin polymer films on a substrate surface. Colloidal particles with glass transition temperature (T_g) above the drying temperature are named as hard latex (high T_g) particles. On the other hand, a colloidal particle with T_g below the drying temperature is called as soft latex (low T_g) particles. Studies on the film-forming process of latex polymers represent a field of intense research since many years. A fundamental understanding of the dynamical and mechanical properties of polymer thin films is important in many applications including organic light emitting devices, protective encapsulations in microelectronics, lubricant coatings, and so on. Generally, Film formation from soft and hard latex dispersions can occur in several stages [2–5]. In both cases, the first stage corresponds to the wet initial stage. Evaporation of solvent leads to second stage in which the particles form a close-packed array, here if the particles are soft they are deformed to polyhedrons. Hard latex particles remain essentially discrete and undeformed during drying. The mechanical properties of such films can be evolved after all the solvent is evaporated by annealing process. Annealing of soft particles causes diffusion across particle–particle boundaries that lead to a homogeneous continuous material. In the annealing of hard latex system, however, deformation of particles first leads to void closure [6–8] and then after the voids disappeared diffusion across particle–particle boundaries starts. The last stage of film formation is the coalescence of the particles where macromolecules belonging to different particles mix by interdiffusion [9] and a molecularly homogeneous polymer film is formed.

In last decade, there has been growing interest in producing new materials by filling polymers with inorganic natural and/or synthetic compounds. Because the inorganic particles display rather macroscopic dimensions and there is mostly no interaction between the two mixed components at the interface between the two partners, the resulting composite materials can be seen as filled polymers. By using composites, we can combine two materials to make them better than there components in certain areas or manipulate the components to get a desired result. The prior limitations of each material can be eliminated with the combination of the characteristics among the starting materials. Polymers are great for such properties as there light weight and flexibility. A defining feature of polymer nanocomposites is that the small size of the fillers leads to a dramatic increase in interfacial area

Correspondence to: Saziye Ugur; e-mail: saziye@itu.edu.tr
Contract grant sponsor: Turkish Academy of Sciences (TUBA; OP).
DOI 10.1002/pen.23560
Published online in Wiley Online Library (wileyonlinelibrary.com).

as compared with traditional composites. This interfacial area creates a significant volume fraction of interfacial polymer with properties different from the bulk polymer even at low loadings [10–14]. Inorganic nanoscale building blocks include nanotubes, layered silicates (e.g., montmorillonite, saponite), nanoparticles of metals (e.g., Au, Ag), metal oxides (e.g., TiO_2, Al_2O_3), semiconductors (e.g., PbS, CdS), and so forth.

Spontaneously organized colloidal crystals have been widely used as three-dimensional (3D) templates for the construction of macroporous materials. This macroscale templating approach typically consists of three steps. First, the interstitial voids of the monodisperse sphere arrays are filled with precursors of various classes of materials, such as metals [15, 16], semiconductors [17, 18], ceramics [19, 20], monomers [21, 22], and so on. In the second step, the precursors condense and form a solid framework around the spheres. Finally, the spheres are removed by either calcination or solvent extraction leading to the formation of 3D-ordered air cavities inside the void-filling materials. 3D-ordered polymeric nanocomposites have also found important technological applications ranging from photonic papers [23] to ultrahigh-density optical recording materials [24]. In the last few years, templating methods have proved successful for the design of hierarchical porosity [25] as the size of the templating beads could be modified. Surfactant arrays [25, 26] and emulsion droplets [27, 28] or particles [29, 30] have been used as templates and a wide range of structured porous materials have been prepared including inorganic oxides [29–31], carbons [32], metals [33], and polymers [34].

Ordered arrays of polymer [e.g., polystyrene (PS) or poly(methyl methacrylate)] or silica nanospheres have been extensively studied in recent years for photonic crystal applications [19, 35–38]. Such systems can be used as the "host" for chemically or electrochemically immobilizing semiconductor particles. Thus, the pores and voids of the ordered matrix can be filled with a metal, semiconductor, or both, which act as the "guest" material. The guest follows the symmetry layout of the voids or pores in the host matrix by self-organization, resulting in the formation of a 3D array nanoarchitecture. Importantly, the macroporous films retain the periodicity of the templates and exhibit strong photonic band gaps that can be tuned by varying the template diameter. Photonic crystals are periodic dielectric arrangements on the optical wavelength scale [39] such as natural opals or highly ordered macroporous substances. The periodic structure of the material leads to strong multiple scattering of light or to a strong modification of wave propagation. Because the lattice constant of photonic crystals is in the visible or infrared wavelength range, they can control the propagation of photons in a way similar to the way a semiconductor does for electrons. Many studies have been carried out to predict and produce the 3D complete photonic band gap structures because of their wide potential applications in optics [39]. Recently, they have attracted renewed interest, mainly because they provide a much simpler, faster, and cheaper approach than complex semiconductor nanolithography techniques to create 3D photonic crystals working in the optical wavelength range [40–42].

In this report, we provide a detailed account of film-formation properties and the morphology of PS/TiO_2 nanocomposites as a function of the thickness of the PS template and TiO_2 content using a combination of spectroscopic and scanning electron microscopy (SEM) methods. PS latex has been selected as the templating entities in the present study, because they can be obtained in a wide variety of sizes and with different functional groups. It is readily available in industrial grade and it has good thin film-forming properties. It is not soluble in water but can easily soluble in organic solvents such as toluene, chloroform, and acetone. These particles also easily form highly ordered films [43], which enables us to prepare ordered porous solids and to control the size of the cavities induced in the matrix. TiO_2 is one of the most common materials that have a great attention with its unique properties. Wide range of application areas includes self cleaning coatings, water purification or water treatment, solar energy cells, and gas sensors. Moreover, TiO_2 is one of the most important photocatalytic materials with its ability to catalyze the degradation of many organic materials. In our previous work [43], we have demonstrated the feasibility of utilizing PS latex spheres as templates to form macroporous TiO_2 films [43]. In the present study, we first investigated the effect of TiO_2 content and thickness of PS templates on film-formation process of PS/TiO_2. In order to study film-formation process, PS/TiO_2 films were annealed in the temperature range of 100–280°C, fluorescence and transmitted light intensities were meausered after each annealing step. Film-formation stages were modeled and related activation energies were calculated. After completion of film formation, to get ordered macroporous TiO_2 thin films, PS was removed by extraction.

EXPERIMENTAL

Materials

Latex Dispersions. The latex samples used in this study are composed of pyrene (P) labeled PS. Fluorescent PS latexes were produced via emulsion polymerization process [44]. The polymerization was performed batch-wisely using a thermostatted reactor equipped with a condenser, thermocouple, mechanical stirring paddle and nitrogen inlet. Water (50 ml), styrene monomer (3 g; 99% pure from Janssen) and the 0.014 g of fluorescent 1-pyrenylmethyl methacrylate (PolyFluor® 394) were first mixed in the polymerization reactor where the temperature was kept constant (at 70°C). The water soluble radical initiator potassium persulfate (1.6%, wt./wt. over styrene) dissolved in small amount of water (2 ml) was then introduced in order to induce styrene polymerization. Surfactant sodium dodecyl sulfate (0.075%, wt./vol.) was added in the

polymerization recipe. The polymerization was conducted under 400 rpm agitation during 12 h under nitrogen atmosphere at 70°C. The particle size was measured using Malven Instrument NanoZS. The mean diameter of these particles is 324 nm. The weight-average molecular weights (M_w) of individual PS chain (M_w) were measured by gel permeation chromatography and found ranging as 3.32×10^5 g mol^{-1}. Glass transition temperature (T_g) of the PS latexes was determined using differential scanning calorimeter and found to be around 105°C.

TiO_2 Solution. TiO_2 sol was prepared at room temperature in the following way: 1.2 ml titanium(IV) butoxide was injected slowly in 15 ml ethanol. A few drop of acetic acid was added and stirred for half an hour. Later, 10 ml ethanol was added to this mixture and stirred for 1 h.

Preparation of PS/TiO_2 Films

First, the glass substrates (0.8 cm × 2.5 cm) were cleaned ultrasonically in acetone and deionized water, respectively. Then, seven different films (PS templates) were prepared from the dispersion of PS particles in water. The PS latexes were assembled on clean glass substrates by casting method by placing the same number of drops on glass substrates. Upon slow drying at room temperature, a dry film of ordered PS spheres was produced. The thickness of the PS templates could be controlled by changing the amount of PS latex spheres suspension deposited. In order to evaluate the film-formation properties depending on the thickness of PS template, two different sets of PS films with 5 μm and 20 μm were prepared. TiO_2 sol was filled into the PS templates by dip-coating method. The PS covered glass substrate is settled vertically into the TiO_2 sol for two min, drawn out and dried at 100°C for 10 min. Here, the TiO_2 content in the films could be adjusted by dipping cycle; and therefore, to investigate the effect of TiO_2 content, the consecutive dipping was performed. When the templates were immersed into the TiO_2 sol, the TiO_2 precursor could permeate the close-packed arrays of PS by capillary force and form a solid skeleton around the PS spheres. Seven different films for each set of films were produced with 0, 5, 8, 10, 12, 13, and 15 layers of TiO_2. In order to study the film-formation behavior of PS/TiO_2 composites, the produced films were separately annealed above T_g of PS, 105°C for 10 min at temperatures ranging from 100 to 280°C. The temperature was maintained within ±2°C during annealing.

Finally, after film-formation process of PS latexes completed, the PS phase was dissolved away in toluene for 24 h, leaving the TiO_2 film with the nanoholes in it.

METHODS

Fluorescence Measurements

After annealing, each sample was placed in the solid surface accessory of a Perkin-Elmer Model LS-50 fluorescence spectrometer. Pyrene (P) was excited at 345 nm and scattered light and fluorescence emission were detected between 300 and 500 nm. All measurements were carried out in the front-face position at room temperature. Slit widths were kept at 8 nm during all steady state fluorescence (SSF) measurements.

Photon Transmission Measurements. Photon transmission experiments were carried out using Variant Carry-100 Bio-UV–Visible (UVV) scanning spectrometer. The transmittances of the films were detected at 500 nm. A glass plate was used as a standard for all UVV experiments, and measurements were carried out at room temperature after each annealing processes.

SEM Measurements. Scanning electron micrographs of the PS/TiO_2 films were taken at 10–20 kV in a JEOL 6335F microscope. A thin film of gold (10 nm) was sputtered onto the surface of samples using a Hummer-600 sputtering system to help image the PS/TiO_2 films against the glass background.

RESULTS AND DISCUSSIONS

Figures 1 and 2 show fluorescence (I_P), scattered (I_{sc}), and transmitted light intensities (I_{tr}) versus annealing temperatures for both thick and thin pure PS films with no TiO_2 content, respectively. Upon annealing, the transmitted light intensity, I_{tr}, started to increase above a certain onset temperature, called the minimum film-formation temperature T_0, for all film samples. Scattered light intensity showed a sharp increase at the single temperature named as the void closure temperature, T_v. Here, we have to mention that I_{sc} is scattered from below the surface as well as from the surface of the latex film; however, I_{tr} goes through the film all the way. Fluorescence intensity I_P first, increase, reach a maximum, and then decrease with increasing annealing temperature. The temperature where I_P reaches the maximum is called the healing temperature, T_h. This temperature is the indication of the particle–particle adhesion. The increase in I_{tr} above T_0 can be explained by the evaluation of the transparency of the PS films upon annealing. Before annealing, since the film contains many voids (i.e., the high number of polymer–air boundaries) most of the light is scattered at the air–polymer interface (surface scattering). Annealing the films first causes the closure of voids due to the viscous flow of PS polymer and then healing of the particle–particle boundaries [45, 46]. Therefore, I_{tr} increases with annealing temperature as shown in Figs. 1 and 2. Furthermore, annealing at higher temperature causes healing and interdiffusion processes [45, 46], resulting in a more transparent film. After the film-formation process is completed (disappearance of voids), scattering takes place predominantly from the PS-TiO_2 boundaries.

The sharp increase in I_{sc} occurs at T_v, which overlaps the inflection point on the I_{tr} curve. Below T_v, light

 DOI 10.1002/pen

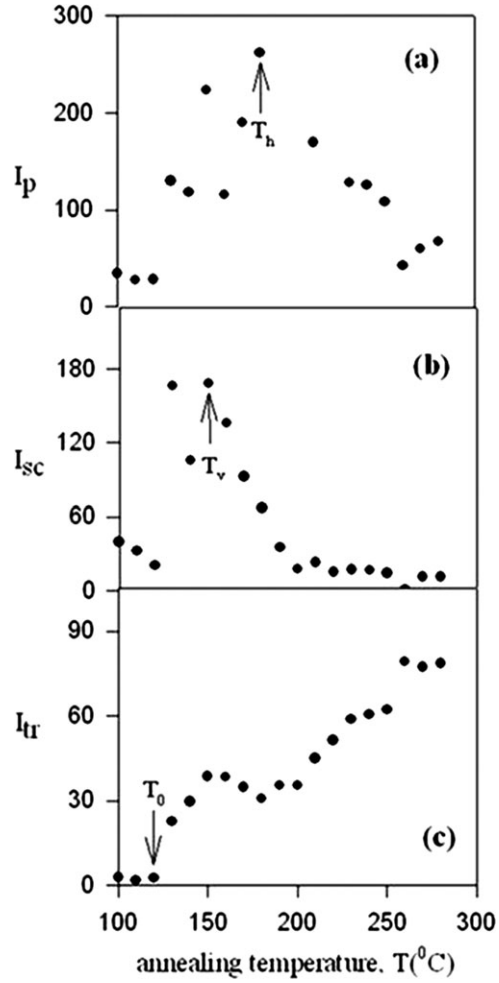

FIG. 1. Plot of (a) I_P, (b) I_{sc}, and (c) I_{tr} intensities of thick PS film versus annealing temperature, T. T_h is the healing temperature, T_v is the void closure temperature, and T_0 is the minimum film-formation temperature.

scatters isotropically because of the rough surface of the PS films. Annealing of the film at T_v creates a flat surface on the film, which acts like a mirror. As a result, light is reflected to the photomultiplier detector of the spectrometer. Furthermore, annealing makes the PS film totally transparent to light and I_{sc} drops to its minimum. On the other hand, the increase in I_P above T_0 presumably corresponds to the void closure process up to the T_h point where the healing process takes place. Decrease in I_P above T_h can be understood by interdiffusion processes between polymer chains [45, 46].

I_P, I_{sc}, and I_{tr} curves of thick and thin PS/TiO_2 composite films for various TiO_2 layer content annealed at various temperatures are also shown in Figs. 3 and 4, respectively. It is clear that all curves shows similar behaviors with the pure PS films in Figs. 1 and 2. This result shows that PS latexes in composite films undergo complete film-formation process. The behavior of T_0, T_v, and T_h values measured for two sets of film reported in Table 1 support these findings. Minimum film formation (T_0), void closure (T_v), and healing (T_h) temperatures are important characteristic related to the film-formation properties of latexes. T_0 is often used to indicate the lowest possible temperature for particle deformation sufficient to decrease interstitial void diameters to sizes well below the wavelength of light [47]. Below this critical temperature, the dry latex is opaque and powdery. However, at and/or above this temperature, a latex cast film becomes continuous and clear film [48]. Therefore, T_0 has been considered in this study as the temperature above which the I_{tr} starts to increase. Here, T_v is the lowest temperature at which I_{sc} become highest and defined as the maxima of the I_{sc} curve. The healing temperature (T_h) is the minimum temperature at which the latex film becomes continuous and free of voids. The healing point indicates the onset of the particle–particle adhesion [48]. Here, T_h is defined as the maxima of the I_P curves versus temperature. From Table 1, the T_0, T_v, and T_h temperatures are about 120–160°C, 150–240°C, and 180–230°C for the thick films, 110–150°C, 130–180°C, and 160–200°C for the thin films, respectively. T_0, T_v, and T_h do not change so much within

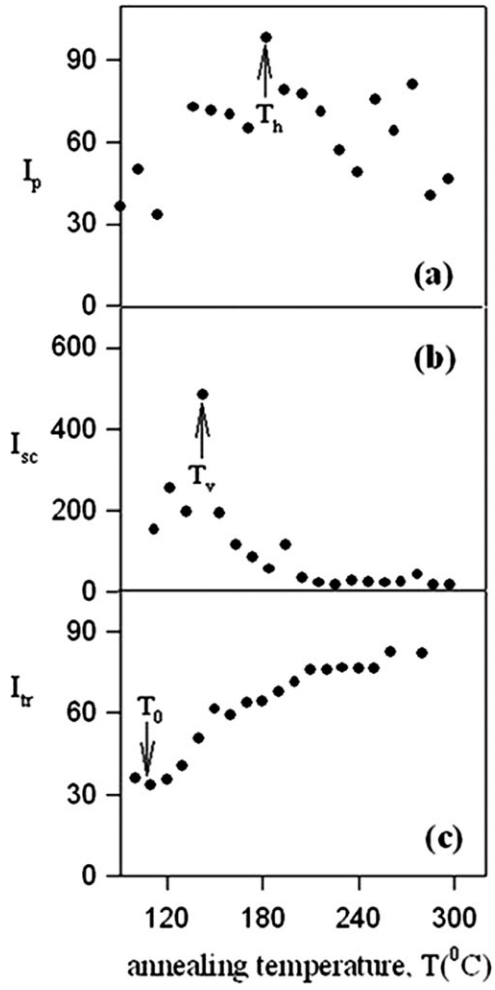

FIG. 2. Plot of (a) I_P, (b) I_{sc}, and (c) I_{tr} intensities of thin PS film versus annealing temperature, T. T_h is the healing temperature, T_v is the void closure temperature, and T_0 is the minimum film-formation temperature.

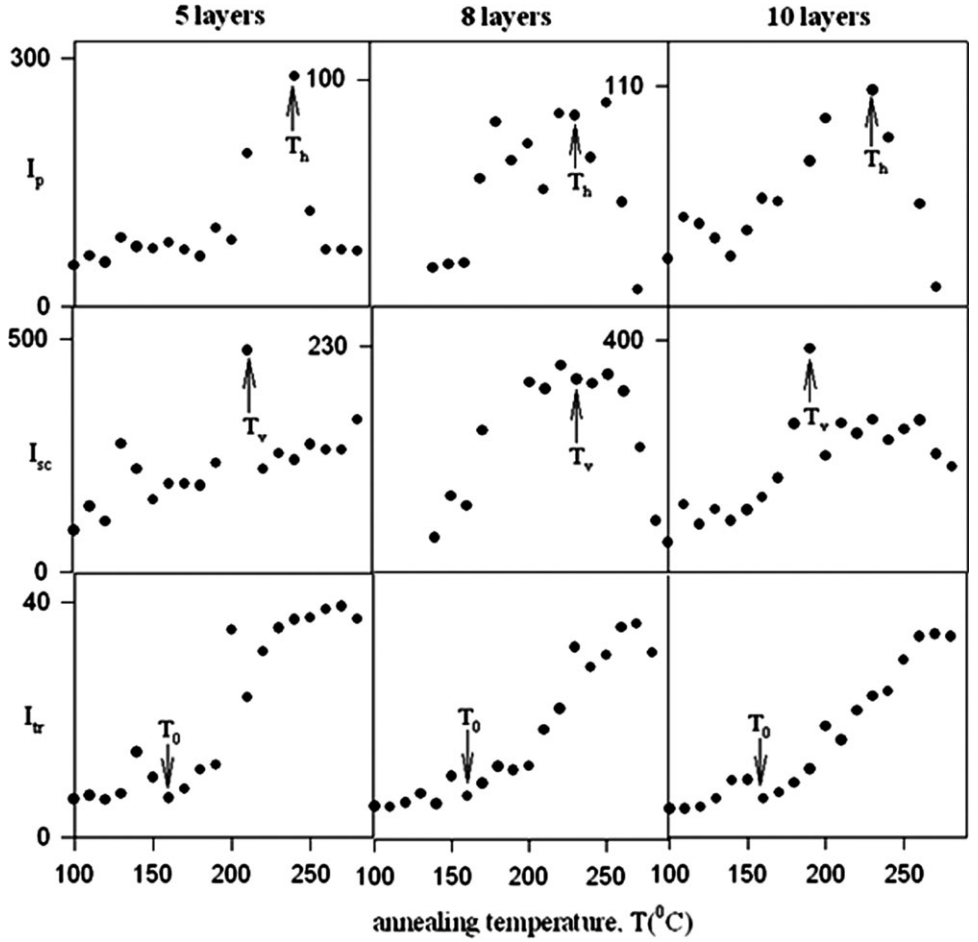

FIG. 3. Plot of I_P, I_{sc}, and I_{tr} intensities versus annealing temperature, T for the thick composite films for various TiO_2 layers. Numbers on each curve shows TiO_2 layer.

the each series with TiO_2 content but are all shifted to higher temperatures with the thickness of the PS template. This point out that film formation by PS latex polymers in thick films is retarded, compared to thin films. As a result, film formation of PS latexes was strongly influenced by the film thickness.

The behavior of I_P and I_{tr} during annealing is schematically presented in Fig. 5 for a film with TiO_2 [43, 49, 50]. In Fig. 5a, film posses many voids, which results in short mean free and optical paths of a photon yielding very low I_P and I_{tr}. Figure 5b shows a film in which interparticle voids disappear due to annealing, which gives rise to a long mean free and optical path in the film. At this stage, I_P and I_{tr} reach its maximum values. Finally, Fig. 5c presents almost transparent film with no voids but some TiO_2 background. At this stage, film has low I_P but high I_{tr} because the mean free path is very long but the optical path is short.

Film-Formation Mechanisms

Void Closure. In order to quantify the behavior of I_P in Figs. 1–4, below T_h and above T_0, a phenomenological void closure model can be introduced. Latex deformation and void closure between particles can be induced by shearing stress which is generated by surface tension of the polymer, that is, polymer–air interfacial tension. The void closure kinetics can determine the time for optical transparency and latex film formation [51]. In order to relate the shrinkage of spherical void of radius, r, to the viscosity of the surrounding medium, η, an expression was derived and given by the following relation [51].

$$\frac{dr}{dt} = \frac{\gamma}{2\eta}\left(\frac{1}{\rho(r)}\right) \tag{1}$$

where γ is the surface energy, t is time, and $\rho(r)$ is the relative density. It has to be noted that here the surface energy causes a decrease in void size and the term $\rho(r)$ varies with the microstructural characteristics of the material, such as the number of voids, the initial particle size, and packing. *Equation 1* is similar to one that was used to explain the time dependence of the minimum film-formation temperature during latex film formation [52, 53]. If the viscosity is constant in time, integration of *Eq. 1* gives the relation as

 DOI 10.1002/pen

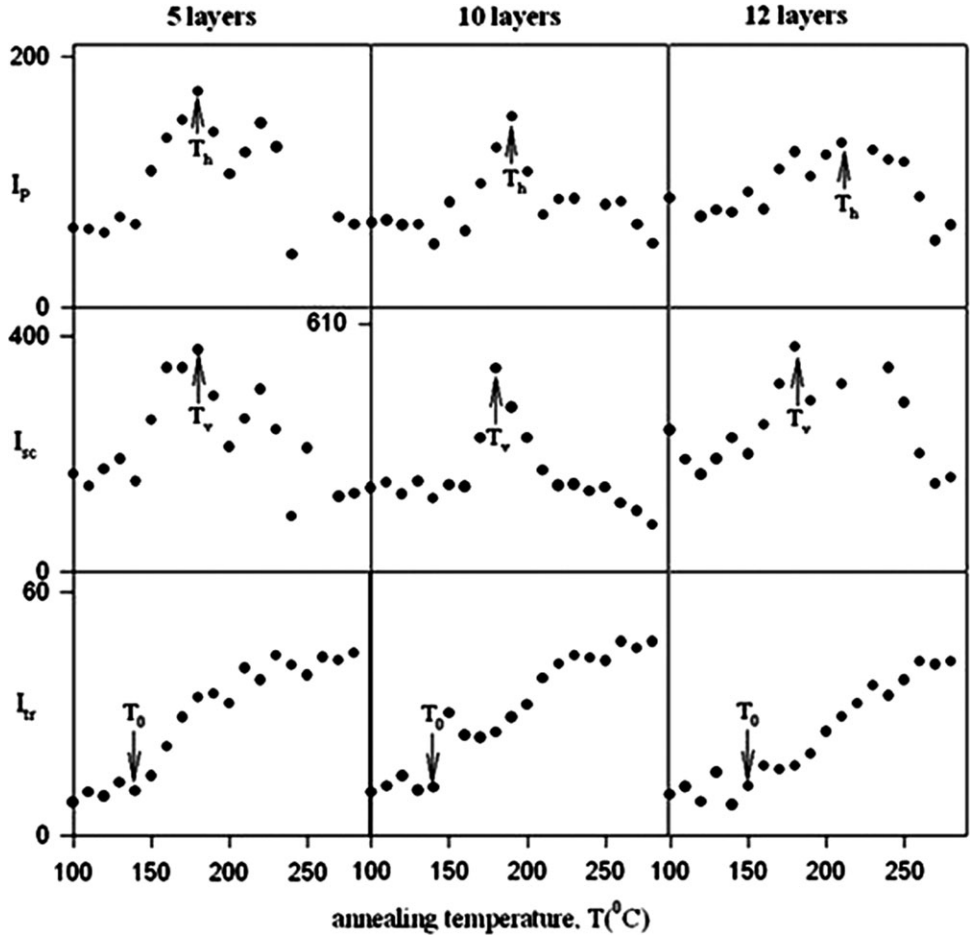

FIG. 4. Plot of I_P, I_{sc}, and I_{tr} intensities versus annealing temperature, T for the thick composite films for various TiO_2 layers. Numbers on each curve shows TiO_2 layer.

$$t = -\frac{2\eta}{\gamma}\int_{r_0}^{r}\rho(r)dr \tag{2}$$

where r_0 is the initial void radius at time $t = 0$. The dependence of the viscosity of polymer melt on temperature is affected by the overcoming of the forces of macromolecular interaction, which enables the segments of polymer chain to jump over from one equilibration position to another. This process happens at temperatures at which

TABLE 1. Minimum film formation (T_0), void closure (T_v), and healing (T_h) temperatures for both thick and thin film sets.

TiO_2 layer	Thick films (20 μm)			Thin films (5 μm)		
	T_0 (°C)	T_v (°C)	T_h (°C)	T_0 (°C)	T_v (°C)	T_h (°C)
0	120	150	180	110	130	180
5	160	210	220	140	180	180
8	160	230	230	150	180	180
10	160	190	220	140	180	190
12	150	220	230	150	180	200
13	140	200	180	120	170	160
15	130	240	230	120	180	200

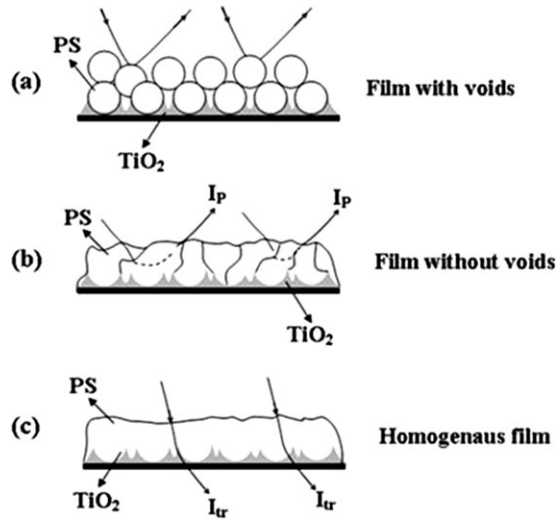

FIG. 5. Cartoon representation of the composite films with TiO_2 at several annealing steps: (a) film posses many voids that results in very low I_P and I_{tr}, (b) interparticle voids disappear due to annealing I_P reaches its maximum value, and (c) transparent film with no voids but some TiO_2 background and has low I_P but high I_{tr}.

the free volume becomes large enough and is connected with the overcoming of the potential barrier. Frenkel–Eyring theory produces the following relation for the temperature dependence of viscosity [54, 55]

$$\eta = \frac{N_0 h}{V}\exp(\frac{\Delta G}{kT}) \tag{3}$$

where N_0 is Avogadro's number, h is Planck's constant, V is molar volume, and k is Boltzmann's constant. It is known that $\Delta G = \Delta H - T\Delta S$, so *Eq. 3* can be written as

$$\eta = A\exp(\frac{\Delta H}{kT}) \tag{4}$$

where ΔH is the activation energy of viscous flow, that is, the amount of heat which must be given to one mole of material to create the act of a jump during viscous flow; ΔS is the entropy of activation of viscous flow. Here, A represents a constant for the related parameters that do not depend on temperature. Combining *Eqs. 2* and *4*, the following useful equation is obtained

$$t = -\frac{2A}{\gamma}\exp(\frac{\Delta H}{kT})\int_{or}^{r}\rho(r)dr \tag{5}$$

In order to quantify the above results, *Eq. 5* can be used by assuming that the interparticle voids are equal in size and the number of voids stays constant during film formation (i.e., $\rho(r)\approx r^{-3}$), Then integration of *Eq. 5* gives the relation

$$t = \frac{2AC}{\gamma}\exp(\frac{\Delta H}{kT})(\frac{1}{r^2} - \frac{1}{r_o^2}) \tag{6}$$

where C is a constant related to relative density $\rho(r)$. As we stated before, decrease in void size (r) causes an increase in I_P. If the assumption is made that I_P is inversely proportional to the sixth power of void radius, r, then *Eq. 6* can be written as

$$t = \frac{2AC}{\gamma}\exp(\frac{\Delta H}{kT})(I^{1/3}) \tag{7}$$

Here, $r_o{}^2$ is omitted from the relation since it is very small compared to r^2 values after the void closure process is started. *Equation 7* can be solved for I_P and I_{tr} ($=I$) to interpret the results in Figs. 1–4 as

$$I(T) = S(t)\exp(-\frac{3\Delta H}{kT}) \tag{8}$$

where $S(t) = (\gamma t/2AC)^3$. For a given time the logarithmic form of *Eq. 5* can be written as follows:

$$\mathrm{Ln}I(T) = \mathrm{Ln}S(t) - \left(\frac{3\Delta H}{kT}\right) \tag{9}$$

As it was already argued above that the increase in both I_P and I_{tr} originate due to the void closure process,

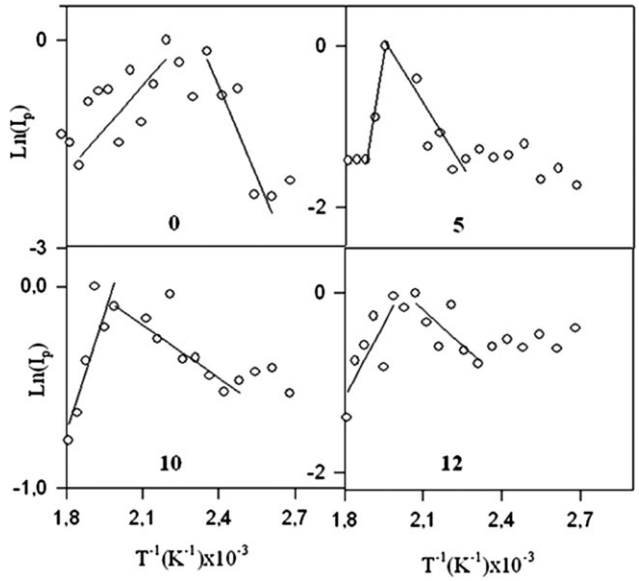

FIG. 6. The ln(I_P) versus T^{-1} plots of the data in Figs. 1 and 3 for the thick composite films with 0, 5, 10, and 12 layers of TiO_2. The slope of the straight lines on right- and left-hand sides of the graph produces ΔH_P and ΔE activation energies, respectively.

then *Eq. 9* was applied to I_{tr} above T_0 and to I_P below T_h for all film samples in two sets. Figures 6 and 7 present the ln I_P versus T^{-1} and Figs. 8 and 9 present ln I_{tr} versus T^{-1} plots for both sets of films from which ΔH_P and ΔH_{tr} activation energies were obtained. The measured ΔH_P and ΔH_{tr} activation energies are listed in Table 2 for both series where it is seen that activation energies do not change much by increasing the TiO_2 layer content and film thickness. The amount of heat that was required by 1 mol of polymeric material to accomplish a jump during viscous flow does not change by varying the layers on the latex films and film thickness. ΔH_P values were found to be slightly smaller than ΔH_{tr} values for both series. This difference most probably originates from different measurement techniques, where the first one measures the film formation from latexes at the surface, however, second one measures the film formation from the iner latexes, which requires higher energies. When comparing the activation energies of both series, it is seen that average ΔH value of thick and thin films is almost the same. This implies that the viscous flow process is not significantly affected by both TiO_2 content and the thickness of PS template. If one compares the ΔH_P values produced in this study with the values produced for pure PS latex system ($\Delta H_P = 8.85$ kcal mol^{-1}) [45], then, one can reach a conclusion that inclusion of TiO_2 into the latex system considerably lowers the viscous flow activation energy ΔH_P. In other words, the existence of TiO_2 promotes the void closure process. As a result, latex film formation can be accomplished with much less energy in composites than in a pure latex system. In addition, the produced ΔH_P values in this study are also smaller than the $\Delta H_P = 6.15$ kcal mol^{-1} value

 DOI 10.1002/pen

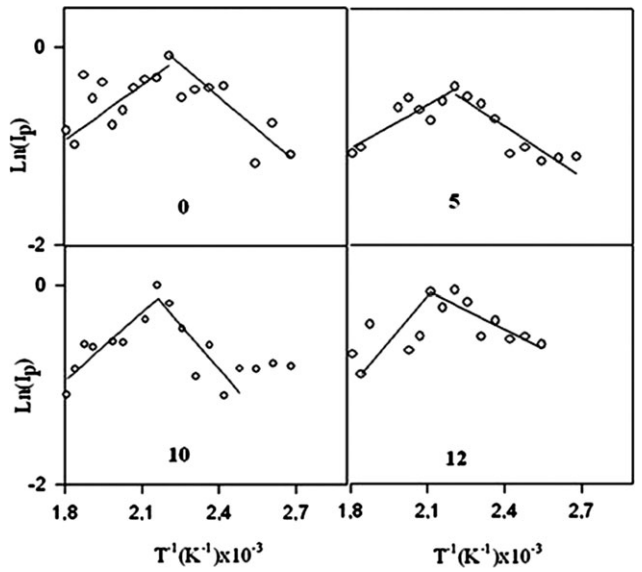

FIG. 7. The $\ln(I_P)$ versus T^{-1} plots of the data in Figs. 2 and 4 for the thin composite films with 0, 5, 10, and 12 layers of TiO_2. The slope of the straight lines on right- and left-hand side of the graph produces ΔH_P and ΔE activation energies, respectively.

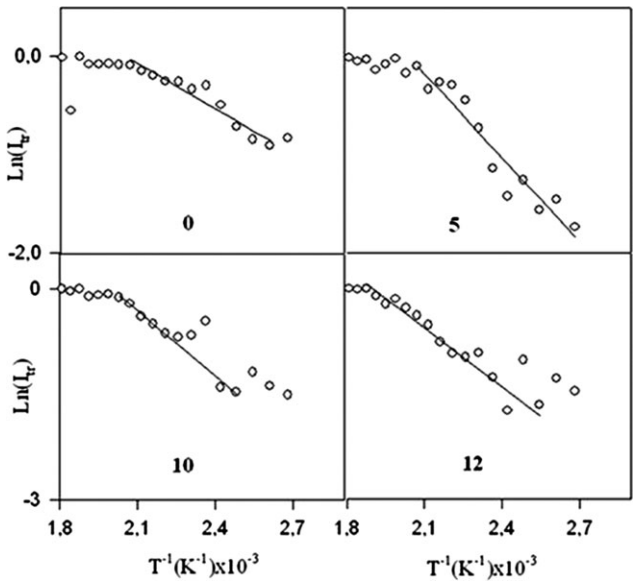

FIG. 9. The $\ln(I_{tr})$ versus T^{-1} plots of the data in Figs. 2 and 4 for the thin composite film contains 0, 5, 10, and 12 layers of TiO_2. The slope of the straight lines produces ΔH_{tr}.

produced in our previous study for PS/TiO_2 films with 1–5 TiO_2 layers [43]. This difference can be explained with the higher (5–15) TiO_2 layer content in this study which prevents PS latex to flow.

Healing and Interdiffusion

The decrease in I_P was already explained in previous section, by interdiffusion of polymer chains. As the annealing temperature is increased above maxima, some part of the polymer chains may cross the junction surface and particle boundaries disappear, as a result I_P decreases due to transparency of the film. In order to quantify these results, the Prager–Tirrell (PT) model [56, 57] for the chain crossing density can be used. These authors used de Gennes's "reptation" model to explain configurational relaxation at the polymer–polymer junction where each polymer chain is considered to be confined to a tube in which executes a random back and forth motion [58]. The total "crossing density" (t) (chains per unit area) at junction surface then was calculated from the contributions $_1(t)$ due to chains still retaining some portion of their initial tubes, plus a remainder $_2(t)$ that is, contribution comes from chains which have relaxed at least once. In terms of reduced time $\tau = 2vt/N^2$ the total crossing density can be written as [9]

$$\sigma(\tau)/\sigma(\infty) = 2\pi^{-1/2}\tau^{1/2} \tag{10}$$

where v and N are the diffusion coefficient and number of freely jointed segment of polymer chain [56].

In order to compare our results with the crossing density of the PT model, the temperature dependence of $\sigma(\tau)/\sigma(\infty)$ can be modeled by taking into account the following Arrhenius relation for the linear diffusion coefficient

$$v = v_o \exp(-\Delta E/kT) \tag{11}$$

Here, E is defined as the activation energy for backbone motion depending on the temperature interval.

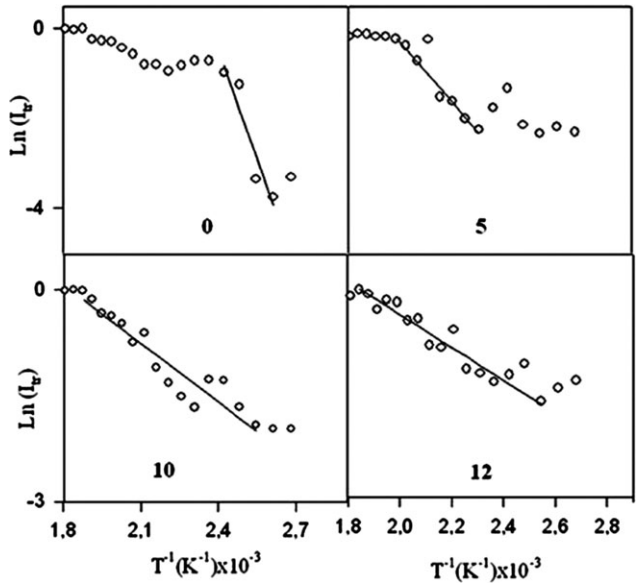

FIG. 8. The $\ln(I_{tr})$ versus T^{-1} plots of the data in Figs. 1 and 3 for the thick composite film contains 0, 5, 10, and 12 layers of TiO_2. The slope of the straight lines produces ΔH_{tr}.

TABLE 2. Experimentally produced activation energies of both thick and thin film sets for varying numbers of TiO_2 layers.

	Thick films (20 μm)			Thin films (5 μm)		
TiO_2 layer	ΔH_P (kcal mol^{-1})	ΔH_{tr} (kcal mol^{-1})	ΔE (kcal mol^{-1})	ΔH_P (kcal mol^{-1})	ΔH_{tr} (kcal mol^{-1})	ΔE (kcal mol^{-1})
0	4.2	7.6	11.8	1.0	0.7	5.2
5	2.4	2.5	53.0	1.1	1.3	5.7
8	0.7	1.6	33.4	1.1	1.7	6.5
10	0.4	1.3	10.8	1.4	1.4	6.3
12	1.2	1.1	15.0	0.6	1.3	8.4
13	0.8	1.2	12.9	2.2	1.9	6.1
15	0.5	1.3	37.7	0.7	0.9	21.6
Average (except 0)	1.0	1.5	27.1	1.2	1.4	9.1

Combining *Eqs. 10* and *11*, a useful relation is obtained as

$$\sigma(\tau)/\sigma(\infty) = R_o \exp(-\Delta E/2kT) \tag{12}$$

where $R_o = (8v_o t/\pi N^2)^{1/2}$ is a temperature independent coefficient. The decrease in I_P in Figs. 1–4 above T_h is already related to the disappearance of particle–particle interface. As annealing temperature increased, more chains relaxed across the junction surface and as a result the crossing density increases. Now, it can be assumed that I_P is inversely proportional to the crossing density $\sigma(t)$ and then the phenomenological equation can be written as

$$I_P(\infty) = R_0^{-1} \exp(\Delta E/2k_B T) \tag{13}$$

The activation energy of backbone motion, ΔE is produced by least-squares fitting the data in Figs. 6 and 7 (the left-hand side) to *Eq. 13* and are listed in Table 2. The average ΔE value for each set does not change with increasing TiO_2 layer indicating that TiO_2 layer content does not affect the backbone motion of

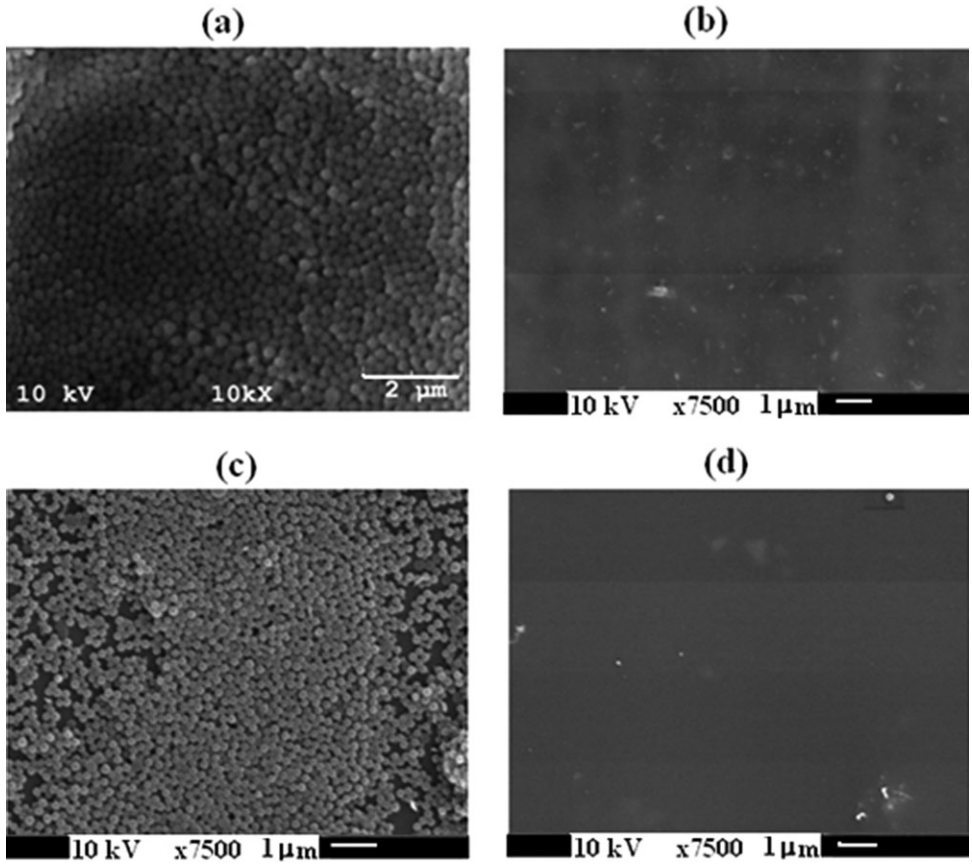

FIG. 10. SEM images of thick and thin films annealed at 100°C (a and c) and 280°C (b and d), respectively.

 DOI 10.1002/pen

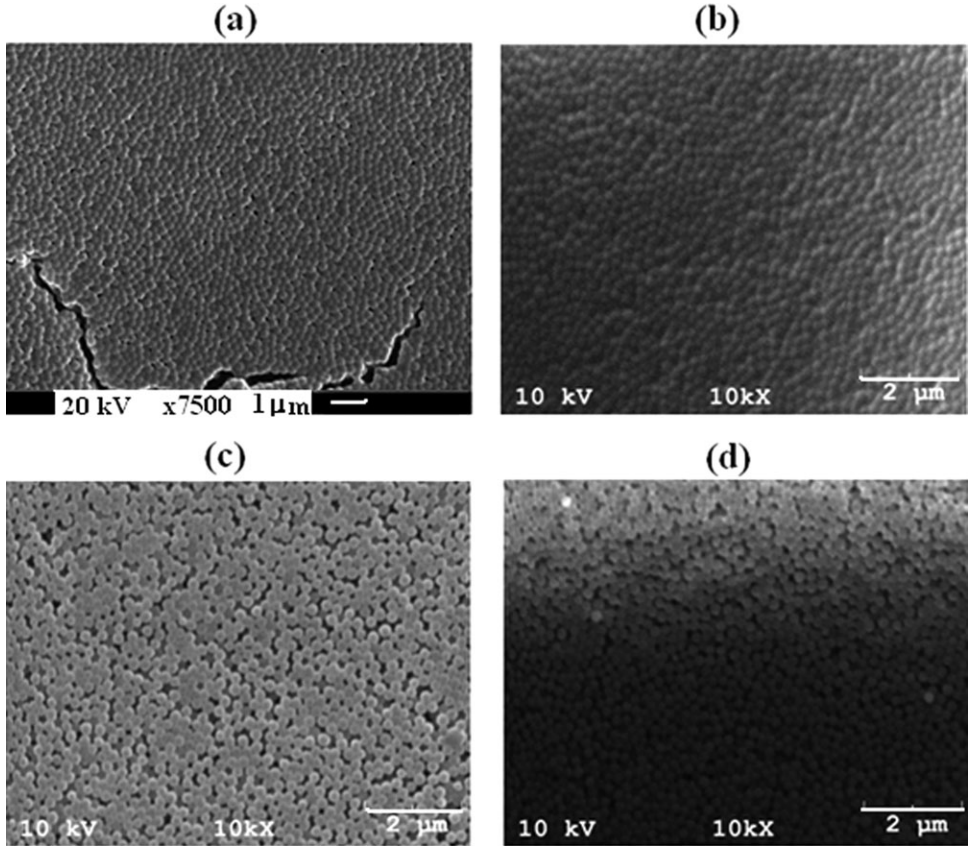

FIG. 11. SEM images of thick PS/TiO_2 films with (a) 5, (b) 8, (c) 10, and (d) 12 TiO_2 layer content annealed at 100°C.

the polymer chains across the junction surfaces. In other words, the film-formation behavior was unaffected by the TiO_2 coating. In addition, average ΔE value of thick samples is almost three times larger than those of thin films. The film thickness evidences that chain confinement effect exists, which may give rise to strong perturbations to chain conformations [59, 60]. It was reported that for sufficiently thick films the bulk mechanism dominates [61] and due to the reduced entanglement of the polymer chains, segmental mobility can be enhanced in thin polymer films. On the other hand, it was shown that the molecular motions near the polymer–air interface are much faster than those in the bulk polymer, due to a reduction in the chain entanglement near the polymer free surface [62–64]. Therefore, the higher activation energy for thick films can be explained by the high density of entanglement (bulk mechanism) which causes the slower motion of polymer chains. Fakhraai and Forrest [65] also found that the activation energy decreasing with decreasing film thickness in consistent with our results. Furthermore, ΔE values are larger than the void closure activation energies for both series. This result is understandable because a single chain needs more energy to execute diffusion across the polymer–polymer interface than to be accomplished by the viscous flow process.

Film Morphology

Figure 10 shows SEM images of thick and thin PS templates annealed at 100°C and 280°C for 10 min, respectively. SEM images of the PS templates show that both films exhibit individual monodisperse particles. The latex particles are randomly distributed and the latex particles still exhibit spherical shapes, and no deformation has occurred. This confirms that particle coalescence and film formation have not yet occurred. After annealing at 280°C (Fig. 10b and c), it is seen that all memory of the original particles are lost and a continuous latex film formed due to the interdiffusion of polymer chains. The SEM pictures presented here show that film formation of PS latexes in pure thin and thick films is completed after annealing at 280°C.

Figs. 11 and 12 show SEM images of thick and thin PS/TiO_2 films coated with 5, 8, 10, and 12 TiO_2 layer annealed at 100°C, respectively. From these figures, we can see some defects at local parts, but consecutive dip-coating cycle seems to lead the formation of an ordered array on a larger area. Here, as well, no deformation of particles was found and the structures of PS colloidal templates are well preserved. After annealing at 280°C (Figs. 13 and 14), as can be seen from SEM images, the PS/TiO_2 films are all compact and smooth. A solid shell

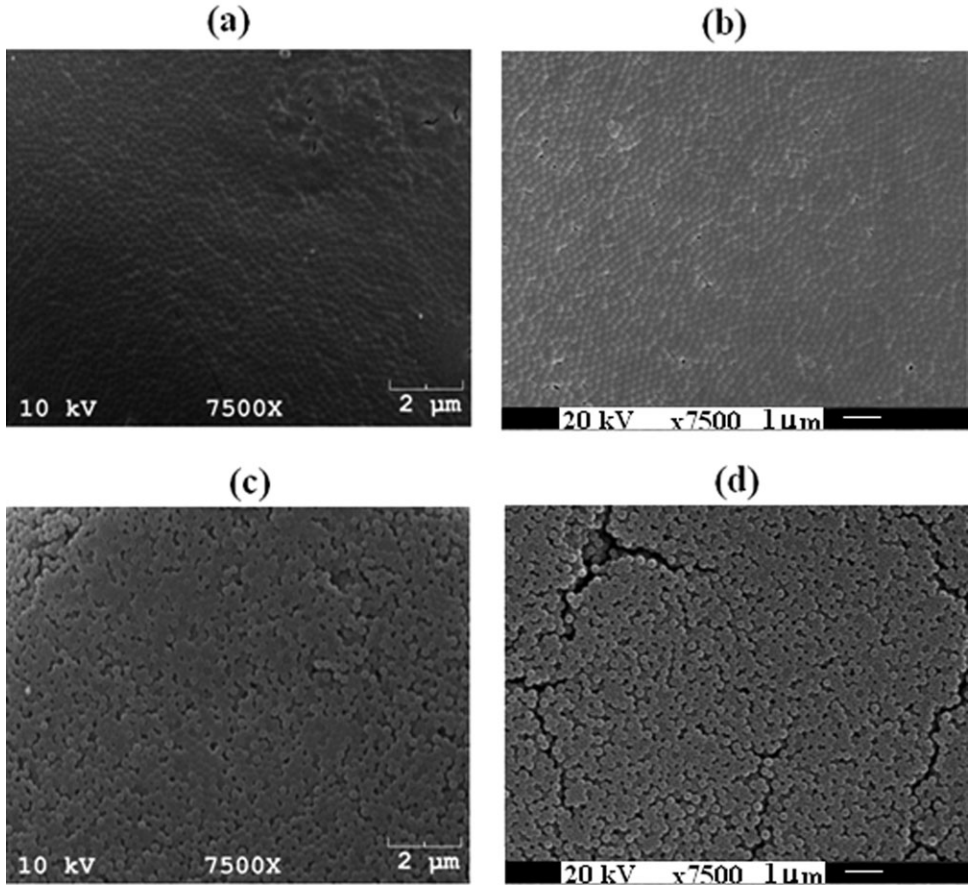

FIG. 12. SEM images of thin PS/TiO_2 films with (a) 5, (b) 8, (c) 10, and (d) 12 TiO_2 layer content annealed at 100°C.

of layer and cracks are seen on the surface of the films in some micrographs. These were likely created during the preparation of composite films for electron microscopy.

In order to determine the extent of film formation, the PS/TiO_2 films were dissolved in toluene for 24 h. Here, toluene was used as the dissolution agent since PS is very soluble in this solvent and the TiO_2 films are stable. Figures 15 and 16 show the influence of TiO_2 concentration on the morphology of thick and thin films after dissolution, respectively. After the PS templates were removed by toluene, the microporous TiO_2 structure formed and remained on the glass site. In case of thick films, PS templates with TiO_2 layers up to eight gave nicely ordered porous films upon dissolution. However, for the films with higher TiO_2 layers (Fig. 15c and d) porous structure cannot be obtained after dissolution because higher concentration results in poor permeation among the close-packed arrays of PS in these films and the TiO_2 coating exhibits a flat top surface. The suitable TiO_2 concentrations that can bring satisfactory permeation to fill the close-packed array of thick PS templates are 5 and 8 layers. So the TiO_2 content is a key for the permeation of thick multilayer templates and plays an important role in the formation of porous films.

Figure 16 shows the SEM images of the thin films after dissolution. As shown in Fig. 16a, the porous structure has primarily been formed but the inorganic wall is thin and nonuniform for 5 layers TiO_2 content film. This indicates that when the content is small TiO_2 precursor cannot fully pour the interstices of PS. TiO_2 sol is easy to fully fill the interstices, but there is not enough solid content when the template is removed. Figure 16b–d shows the morphology of thin films with higher (8–12 layers) TiO_2 content. From these images, it can also be seen that the higher number of dipping cycle, the thicker the pore wall. Moreover, it seems that with increasing TiO_2 content films show a change from a 2D porous structure to a 3D porous structure. However, the level of order and the uniformity of inorganic wall become worse with the increase of dipping cycle.

By means of SEM and fluorescence data, our experiments indicate that all samples present complete film formation and a continuous polymer film with TiO_2 residues for composite systems. In both cases, highly ordered periodic structures of the TiO_2 were obtained after the PS template was removed. However, it is understood that TiO_2 nanoparticles locate mostly within the PS phase for higher TiO_2 content in the thick films, whereas for thin films the TiO_2 particles locate at the interstices of PS latexes which gives nice hole pictures even at higher TiO_2 content.

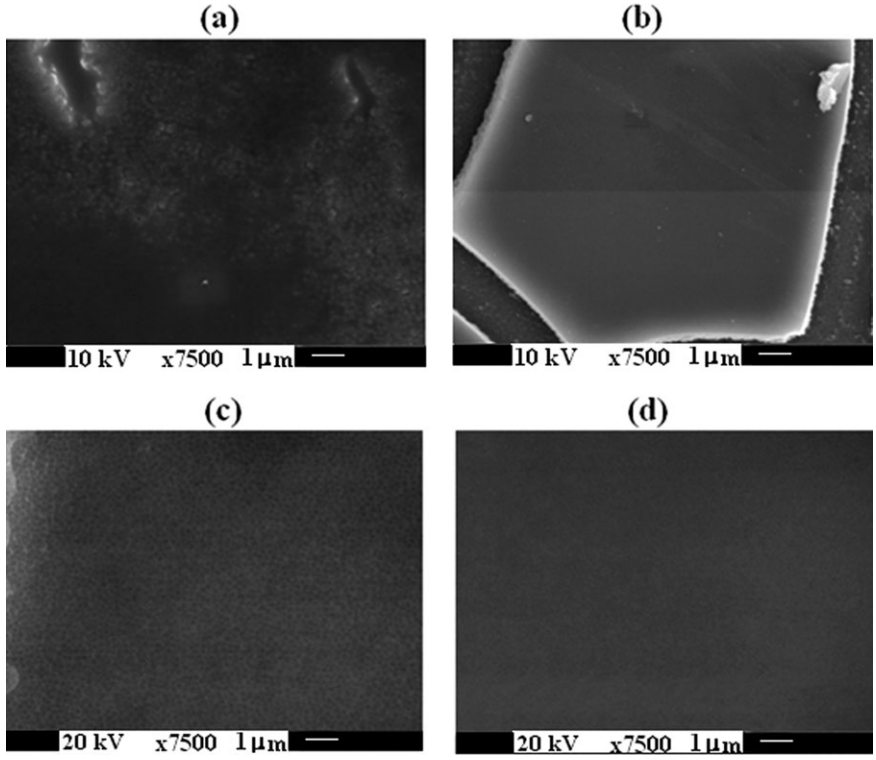

FIG. 13. SEM images of thick PS/TiO_2 films with (a) 5, (b) 8, (c) 10, and (d) 12 TiO_2 layer content annealed at 280°C.

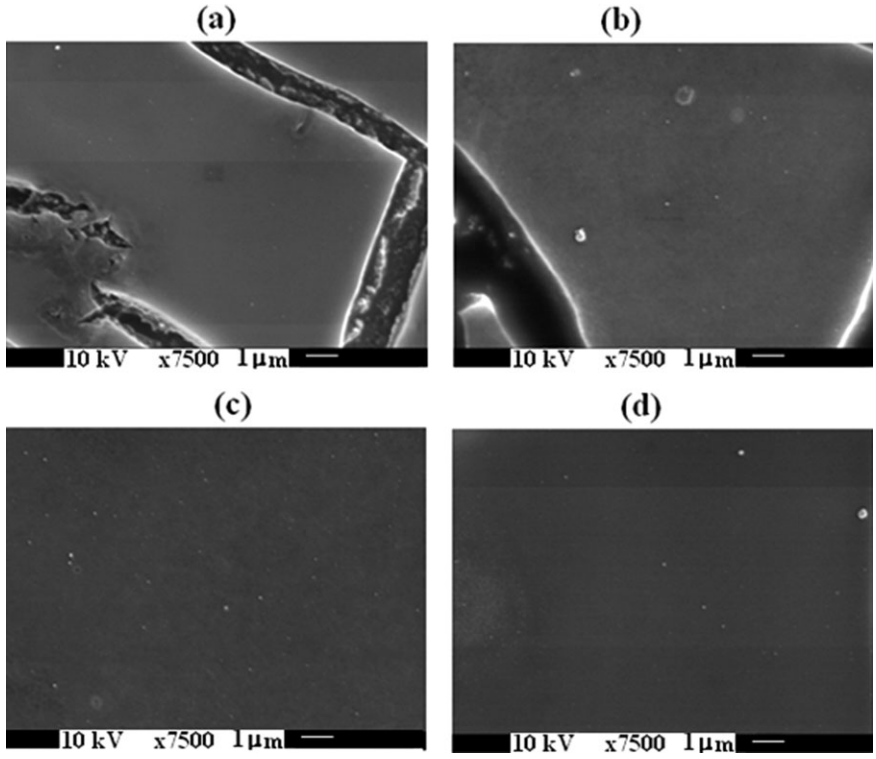

FIG. 14. SEM images of thin PS/TiO_2 films with (a) 5, (b) 8, (c) 10, and (d) 12 TiO_2 layer content annealed at 280°C.

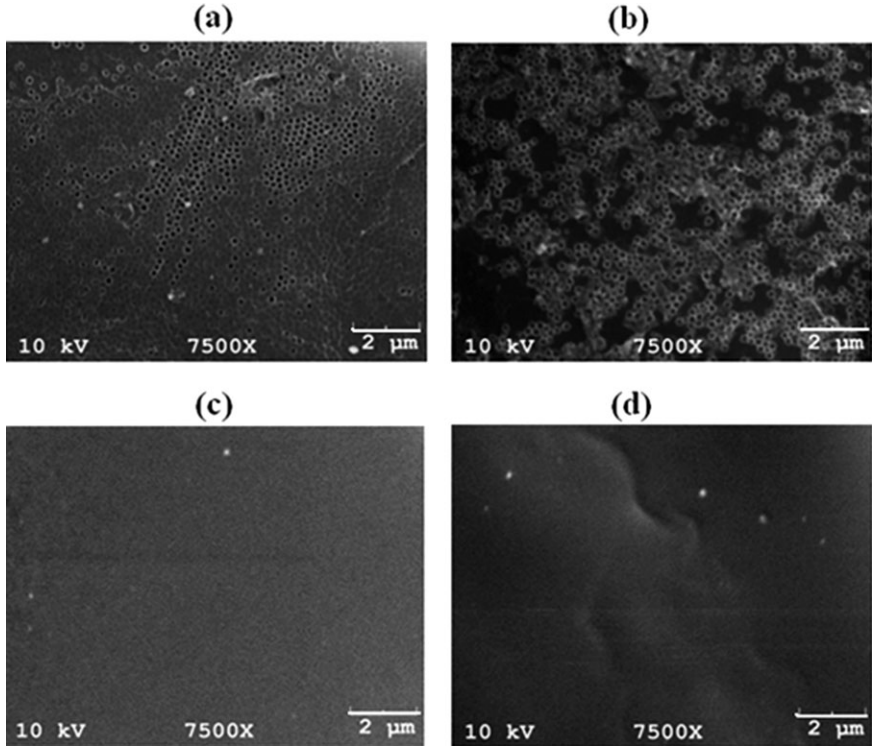

FIG. 15. SEM images of the thick PS/TiO_2 films after extraction of PS template with toluene coated with (a) 5, (b) 8, (c) 10, and (d) 12 TiO_2 layers.

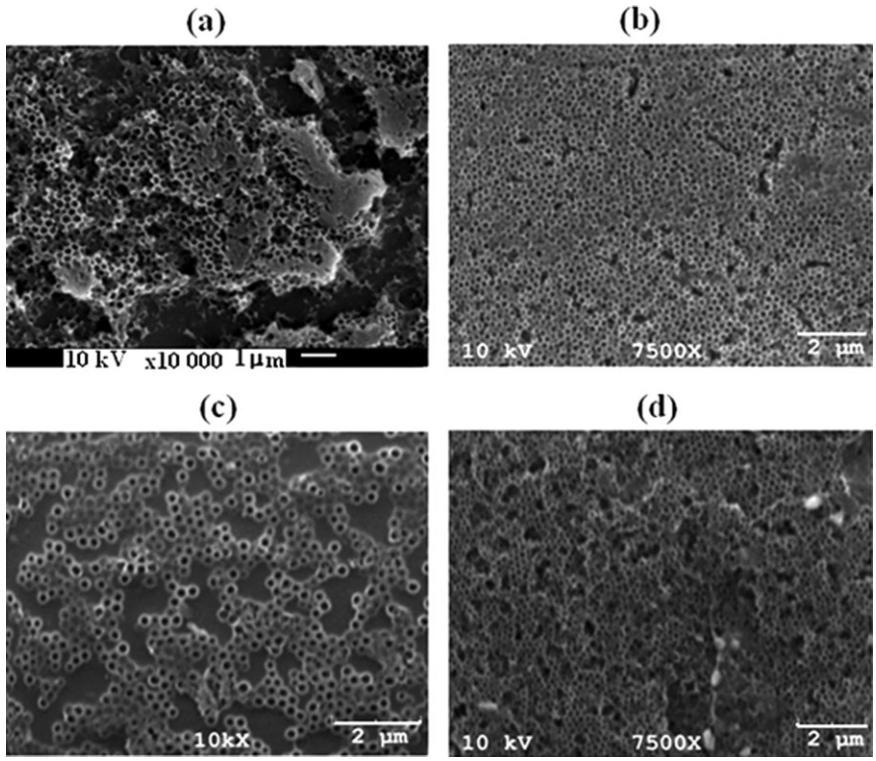

FIG. 16. SEM images of the thin PS/TiO_2 films after extraction of PS template with toluene coated with (a) 5, (b) 8, (c) 10, and (d) 12 TiO_2 layers.

 DOI 10.1002/pen

CONCLUSIONS

We used the SSF technique in conjugation with UVV and SEM techniques to study film-formation process of PS/TiO_2 nanocomposites films and morphological changes depending on PS template thickness and TiO_2 content. The TiO_2 content deposited was precisely controlled via the repeating dipping cycle. The film-formation behavior was unaffected by the TiO_2 coating and a continuous polymer film with TiO_2 residues is observed for all composite systems. These results allow us to conclude that for the PS/TiO_2 composite films, the mechanism of film formation is in good agreement with the pure latex systems. But film thickness has a considerable effect on the film-formation behavior of composite films and their morphology. These findings provide insight into the principle mechanism of latex film formation in inorganic oxide-based building materials. Finally, PS polymer was removed from the composite material by dissolution at room temperature, and the highly ordered porous structures of TiO_2 were obtained. The pore size mainly depends upon the initial size of the microspheres and TiO_2 content, so the dimension of the pores can be fully controlled by varying these two parameters. The ability to vary the dimensions of the walls and those of the pores in a controlled fashion is important in certain applications, such as photonic crystals, so that the periodicity in the dielectric constant can be adjusted. We anticipate that with this strategy, the synthesis of other highly ordered micro–macroporous metal oxide films should also be possible. In our future work, we will expand this method to other metal oxides and PS template with different diameters.

REFERENCES

1. J.K. Keddie, *Mater. Sci. Eng.*, **R21**, 101 (1997).
2. M.A. Winnik, *Curr. Opin. Colloid Interface Sci.*, **2**(**2**), 192 (1997).
3. A. Toussaint and M.D. Wilde, *Prog. Org. Coat.*, **30**, 113 (1997).
4. S.G. Croll, *J. Coat. Technol.*, **58**(**734**), 41 (1986).
5. T. Provder, M.A. Winnik, and M.W. Urban, *ACS Symp., Amer. Chem. Soc. Ser.* **648**, 332 (1996).
6. P.R. Sperry, B.S. Synder, M.L. O'Dowd, and P.M. Lesko, *Langmuir*, **10**(**8**), 2619 (1994).
7. J.K. Mackenzie, and R. Shuttleworth, *Proc. Phys. Soc.*, **B62**(**12**), 838 (1949).
8. S. Mazur, in *Polymer Powder Processing*, N. Rosenweig, Ed., John Wiley and Sons, Chister, England (1995).
9. O. Pekcan and E. Arda, *Colloids Surf. A: Physicochem. Eng. Aspects*, **153**, 537 (1999).
10. A.C. Balazs, T. Emrick, and T.P. Russell, *Science*, **314**, 1107 (2006).
11. R. Krishnamoorti and R.A. Vaia, *J. Polym. Sci., Part B: Polym. Phys.*, **45**(**24**), 3252 (2007).
12. (a) W.R. Caseri, *Mater. Sci. Technol.*, **22**, 807 (2006). (b) W. Caseri, In *Hybrid Materials. Synthesis, Characterization, and Applications*, G. Kickelbick, Ed., Wiley-VCH, Weinheim, Germany, Chapter 2 (2007).
13. (a) L.S. Schadler, *Nanocomposite Science and Technology*; Wiley-VCH, Weinheim, Germany, Chapter 2 (2003). (b) L.S. Schadler, S.K. Kumar, B.C. Benicewicz, S.L. Lewis, and S.E. Harton, *MRS Bull.*, **32**, 335 (2007).
14. D.W. Schaefer, and R.S. Justice, *Macromolecules*, **40**(**24**), 8501 (2007).
15. L.G. Egan, J.S. Yu, C.H. Kim, S.J. Lee, R.E. Schaak, and T.E. Mallouk, *Adv. Mater.*, **12**, 1040 (2000).
16. F. Li, L.B. Xu, W.L. Zhou, J.B. He, R.H. Baughman, and A.A. Zakhidov, *Adv. Mater.*, **14**(**21**), 1528 (2002).
17. Y.A. Vlasov, X.Z. Bo, J.C. Sturm, and D.J. Norris, *Nature*, **414**(**6861**), 289 (2001).
18. Y.A. Vlasov, N. Yao, and D.J. Norris, *Adv. Mater.*, **11**(**2**), 165 (1999).
19. B.T. Holland, C.F. Blanford, and A. Stein, *Science*, **281**, 538 (1998).
20. A. Stein and R.C. Schroden, *Curr. Opin. Solid State Mater. Sci.*, **5**, 553 (2001).
21. S.A. Johnson, P.J. Ollivier, and T.E. Mallouk, *Science*, **283**, 963 (1999).
22. W. Lee, S.A. Pruzinsky, and P.V. Braun, *Adv. Mater.*, **14**, 271 (2002).
23. H. Fudouzi and Y.N. Xia, *Langmuir*, **19**, 9653 (2003).
24. B.J. Siwick, O. Kalinina, E. Kumacheva, R.J.D. Miller, and J. Noolandi, *J. Appl. Phys.*, **90**, 5328 (2001).
25. N. Raman, M.T. Anderson, and C.J. Brinker, *Chem. Mater.*, **8**, 1682 (1996).
26. M.J. Kim and R. Ryoo, *Chem. Mater.*, **11**, 487 (1999).
27. A. Imhof and D.J. Pine, *Nature*, **389**, 948 (1997).
28. V.N. Manoharan, A. Imhof, J.D. Thorne, and D.J. Pine, *Adv. Mater.*, **13**, 447 (2001).
29. O.D. Velev, T.A. Jede, R.F. Lobo, and A.M. Lenhoff, *Nature*, **389**, 447 (1997).
30. B.T. Holland, C.F. Blanford, T. Do, and A. Stein, *Chem. Mater.*, **11**(**3**), 795 (1999).
31. D. Wang, R.A. Caruso, and F. Caruso, *Chem. Mater.*, **13**(**2**), 364 (2001).
32. A.A. Zakhidov, R.H. Baughman, Z. Iqbal, C. Cul, I. Khayrullin, S.O. Dantas, J. Marti, and V.G. Ralchenko, *Science*, **282**(**5390**), 897 (1998).
33. Q. Luo, A. Liu, L. Li, S. Xie, J. Kong, and D. Zhao, *Adv. Mater.*, **13**(**4**), 286 (2001).
34. S.A. Johnson, P.J. Ollivier, and T.E. Mallouk, *Science*, **283**, 963 (1999).
35. T. Yamasaki and T. Tsutsui, *Appl. Phys. Lett.*, **72**, 1957 (1998).
36. Yu.A. Vlasov, K. Luterova, I. Pelant, B. Honerlage, and V.N. Astratov, *Appl. Phys. Lett.*, **71**(**12**), 1616 (1997).
37. A.A. Zakhidov, R.H. Baughman, Z. Ighal, C. Cui, I. Khayrullin, S.O. Dantas, J. Marti, and V.G. Radchenko, *Science*, **282**(**5390**), 897 (1998).
38. Yu.A. Vlasov, N. Yao, and D.J. Norris, *Adv. Mater.*, **11**(**2**), 165 (1999).
39. J.D. Joannopoulos, R.D. Meade, and N. Winn, *Photonic Crystals, Molding the Flow of Light*, Princeton University Press, Princeton, NJ (1995).

40. Y.A. Vlasov, X.Z. Bo, J.C. Sturm, and D.J. Norris, *Nature*, **414**, 289 (2001).
41. A. Blanco, E. Chomski, S. Grabtchak, M. Ibisate, S. John, S.W. Leonard, C. Lopez, F. Meseguer, H. Miguez, J.P. Mondia, G.A. Ozin, O. Toader, and H.M. van Driel, *Nature*, **405**(**6785**), 437 (2000).
42. J. Wijnhoven and W.L. Vos, *Science*, **281**(**5378**), 802 (1998).
43. S. Ugur, S. Sunay, A. Elaissari, F. Tepehan, and O. Pekcan, *Polym. Comp*., **27**(**6**), 651 (2006).
44. J.S. Liu, J.F. Feng, and M.A. Winnik, *J. Chem. Phys*., **101**(**10**), 9096 (1994).
45. S. Ugur, A. Elaissari, and O. Pekcan, *J. Colloid Interface Sci*., **263**(**2**), 674 (2003).
46. S. Ugur, A. Elaissari, and O. Pekcan, *J. Coat. Technol. Res*., **1**(**4**), 305 (2004).
47. J.L. Keddie, P. Meredith, R.A.L. Jones, and A.M. Donald, *Macromolecules*, **28**(**8**), 2673 (1995).
48. S.T. Eckersley and A. Rudin, *J. Coat. Technol*., **62**(**780**), 89 (1990).
49. S. Ugur, S. Sunay, F. Tepehan, and O. Pekcan, *Comp. Interfaces*, **14**(**3**), 243 (2007).
50. M. Canpolat and O. Pekcan, *J. Polym. Sci. Polym. Phys. Ed*., **34**(**4**), 691 (1996).
51. J.L. Keddie, P. Meredith, R.A.L. Jones, and A.M. Donald, in Film Formation in Waterborne Coatings, ACS Symp. Ser., Vol. **648**, T. Provder, M.A. Winnik, and M.W. Urban, Eds., American Chemical Society, 332 (1996).
52. G.B. Mc Kenna, in Comprehensive Polymer Science, Vol. **2**, C. Booth and C. Price, Eds., Pergamon Press, Oxford, UK, **311** (1989).
53. H. Vogel, *Phys. Z*., **22**, 645 (1925).
54. G.S. Fulcher, *J. Am. Ceram. Soc*., **8**, 339 (1925).
55. J. Frenkel, *J. Phys., USSR*, **9**(**5**), 385 (1945).
56. S. Prager and M. Tirrell, *J. Chem. Phys*., **75**(**10**), 5194 (1981).
57. R. P. Wool, B.L. Yuan, and O.J. McGarel, *J. Polym. Eng. Sci*., **29**(**19**), 1340 (1989).
58. P.G. de Gennes, *J. Chem. Phys*., **76**, 3322 (1982).
59. I. Bitsanis and G. Hadziioannou, *J. Chem. Phys*., **92**(**6**), 3827 (1990).
60. J. Baschnagel and K. Binder, *Macromolecules*, **28**(**20**), 6808 (1995).
61. P.G. de Gennes, *Eur. Phys. J. E*., **2**(**3**), 201 (2000).
62. O.K.C. Tsui and H.F. Zhang, *Macromolecules*, **34**(**26**), 9139 (2001).
63. A.M. Mayes, *Macromolecules*, **27**(**11**), 3114 (1994).
64. H. Brown and T.P. Russell, *Macromolecules*, **29**(**2**), 798 (1996).
65. Z. Fakhraai and J.A. Forrest, *Phys. Rev. Lett*., **95**(**2**), 025701 (2005).

 DOI 10.1002/pen